PERGAMON

International Journal of Multiphase Flow 26 (2000) 1281–1294

International Journal of Multiphase Flow

www.elsevier.com/locate/ijmulflow

Gas–liquid two-phase flow patterns and pressure drop in a horizontal micro-rod bundle

T.L. Narrow, S.M. Ghiaasiaan*, S.I. Abdel-Khalik, D.L. Sadowski

G.W. Woodruff School of Mechanical Engineering, Georgia Institute of Technology, Atlanta, 30332-0405 GA, USA

Received 17 August 1998; received in revised form 14 May 1999

Abstract

Two-phase flow patterns and frictional pressure drop in a horizontal micro-rod bundle were experimentally studied, using air and water. The rod bundle was 23 cm long and consisted of seven 3.17-mm diameter rods arranged in a rectangular pattern with 3.71-mm pitch. The rod bundle hydraulic diameter was 1.29 mm. The liquid and gas superficial velocities in the rod bundle center covered the 0.03–5.0 and 0.02–4.0 m/s ranges, respectively. Six distinct flow patterns were observed: bubbly, plug/slug, froth, stratified–intermittent, annular–intermittent and annular. Complete stratification, bundle-wide or in individual subchannels, did not occur. The frictional pressure drops were strongly flow pattern-dependent.

Keywords: Two-phase flow; Microchannel; Rod bundle; Flow patterns; Pressure drop

1. Introduction

Microchannels with hydraulic diameters in the 0.1λ–1.0λ range, with $\lambda = \sqrt{\sigma/g(\rho_L - \rho_G)}$ representing the Laplace length scale (where σ is the surface tension, g is the gravitational acceleration, and ρ_L and ρ_G are the liquid and gas densities, respectively) are of great current interest. The application of microchannels in various miniature cooling systems is expected to grow significantly in the future. Micro-tube bundles can be used as highly efficient miniature heat exchangers and have been considered as the design for the target of the proposed

* Corresponding author.

0301-9322/00/$ - see front matter
PII: S0301-9322(99)00086-5

Accelerator Production of Tritium (APT) system. The objective of the work reported here was to experimentally investigate the gas–liquid two-phase hydrodynamics in a micro-rod bundle.

The two-phase hydrodynamic and heat transfer characteristics of flow channels with hydraulic diameters of the order of or smaller than the Laplace length scale, are known to be significantly different than the characteristics of larger channels. Boiling and two-phase flow in microchannels have been studied rather extensively in the past. Issues that have been addressed, include two-phase flow patterns (Suo and Griffith, 1964; Oya, 1971; Barnea et al., 1983; Damianides and Westwater, 1988; Fukano and Kariyasaki, 1993; Triplett et al., 1999a) two-phase pressure drop (Fukano and Kariyasaki, 1993; Inasaka et al., 1989; Ungar and Cornwell, 1992; Bao et al., 1994; Triplett et al., 1999b), two-phase critical (choked) flow (Amos and Schrock, 1984; John et al., 1988; Ghiaasiaan et al., 1997; Geng and Ghiaasiaan, 1998), and subcooled boiling (Peng et al., 1995). These, and other similar studies, generally confirm that micro-channels have significantly different characteristics than larger channels.

Two-phase flow in rod bundles is of great interest due to its occurrence in nuclear reactors. Current best-estimate system codes applied for nuclear reactor safety analysis often use empirical two-phase flow pattern maps with void fraction and mass flux as parameters (Pasamehmetoglu et al., 1990; RELAP5 Development Team, 1995; Paulson et al., 1996). Two-phase frictional pressure drop in rod bundles, furthermore, is commonly calculated in the best-estimate codes using correlations and methods that are primarily based on experimental data obtained in tubes. These, and other similar correlations evidently may not be appropriate for micro-rod bundles.

Horizontal rod bundles are used as fuel channels in CANDU nuclear reactors and their two-phase hydrodynamic characteristics have been investigated in the past (Aly, 1981; Krishnan and Kowalski, 1984; Osamusali et al., 1992). Partial stratification can readily occur in horizontal rod bundles and can lead to dry out and critical heat flux. The transition from intermittent to stratified flow pattern has therefore been the focus of the aforementioned studies. The results of these studies, however, may not be applicable to micro-rod bundles. Two-phase flow in micro-rod bundles has not been investigated in the past.

2. Experiments

2.1. Apparatus

A schematic of the test loop is displayed in Fig. 1. During experiments, water from the supply tank B, a 110-l stainless steel tank, flows through the pump D, the heat exchanger E, the metering valve G, and from there through either valve I (for low liquid flow rates) or valve J (for high liquid flow rates). Upon leaving the flow meters, water is mixed with air in the air–water mixer U. The objective of the heat exchanger E is to dispose of the heat generated in the booster pump D. The supply tank B can be pressurized by compressed air; however, for all experiments reported here, ambient conditions were maintained on top of the water free surface. Compressed air from a house line passes through the oil filter S and the regulator N, and prior to entering the air–water mixer U, it flows through a series of flow meters and the

filter L. The air–water mixture leaving the test bundle, T, is discharged into the collection tank P.

The air–water temperature and pressure are measured near the test section inlet by thermocouple 10 and the absolute pressure transducer 9. The pressure difference between the test section inlet and outlet is measured by the differential pressure transducer 11.

The cross-sectional configuration of the rod bundle is displayed in Fig. 2. The rods form six inner subchannels (subchannels 1–6), representative of rod bundles with triangular arrays, and six peripheral subchannels (channels 7–12). The hydraulic diameter of the rod bundle is 1.29 mm.

Without appropriate precautions, a rod bundle's entrance effects can be significant due to their abrupt flow area geometry change. Multiple rod bundles configured in series, with two or more bundles placed upstream of the instrumented rod bundle, in order to eliminate entrance effects, have previously been used (Krishnan and Kowalski, 1984; Osamusali et al., 1992). Due to the very large pressure drops in micro-rod bundles, however, multi-rod bundles in series are impractical. Extraordinary precautions were applied in the design of the test bundle ends, in

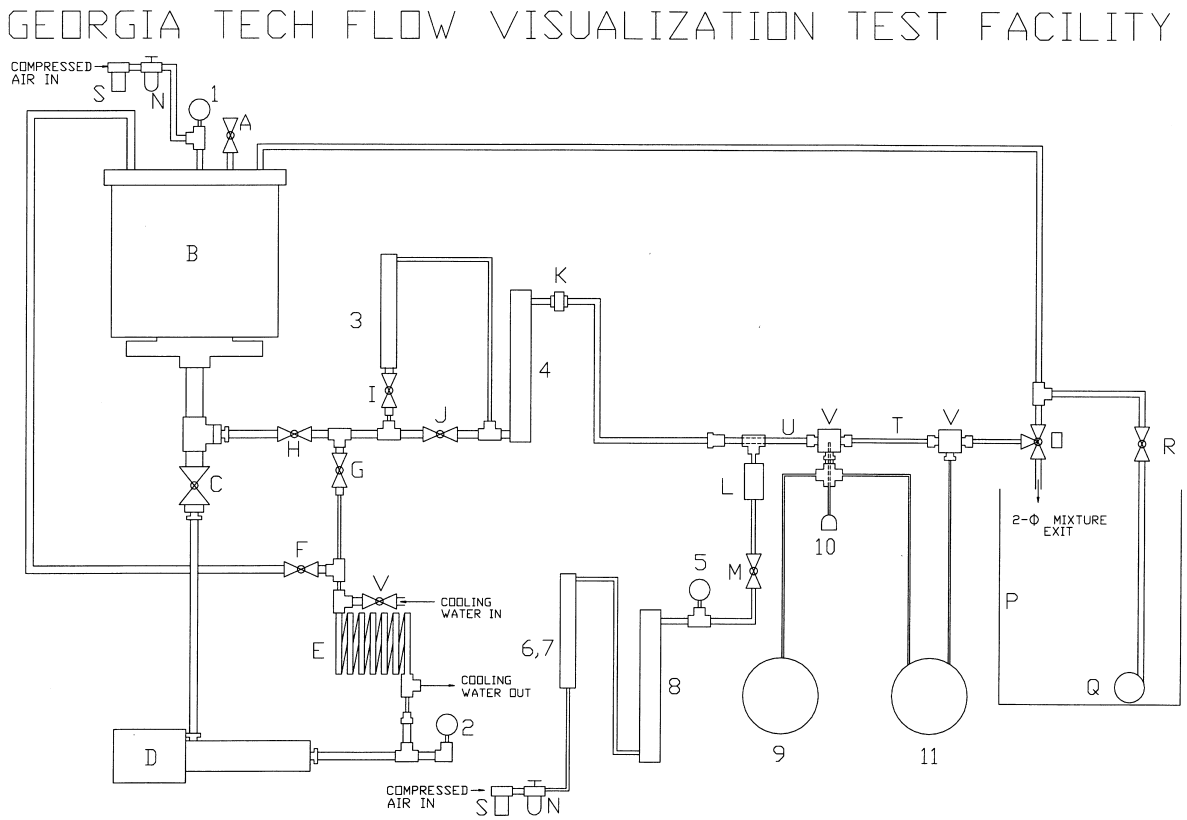

Fig. 1. The test loop. (B = stainless steel supply tank; D = booster pump; E = heat exchanger; G = metering valve; N = regulator; P = collection tank; S = compressed-air oil filter; T = test section; U = mixer; 1, 2, 5 = pressure gauges; 3.4 = water rotameters; 5, 6, 7, 8 = air rotameters; 9 = absolute pressure transducer; 10 = thermocouple; 11 = differential pressure transducer.)

order to minimize its end effects. Before entering the test section, the air–water mixture passes through a short 10.31 mm-inner diameter cylindrical channel; a Teflon cap with six parallel holes; an annular flow channel 5.7 mm long with 3.18 mm and 10.64 mm inner and outer diameters, respectively; and a steel-end cap with 12 holes, each 1.59 mm in diameter. When the test rod bundle is installed, these 12 small through holes become aligned with the 12 interstitial subchannels in the rod bundle. The purpose of these components, all of which reside at the inlet to the test rod bundle, is to minimize the rod bundle entrance effects. The test section exit is similar to its entrance, only in reverse order. Further details can be found in Narrow (1998).

A digital video camera, connected via a parallel port to a personal computer's internal clock, directly viewed subchannels 11 and 12 and subchannels 5 and 6, which were visible through the transparent rod in front of them. All experiments were conducted using air and water at room temperature.

2.2. Calculation of the rod bundle pressure drop

The pressure at rod bundle inlet, P_{in}, must be calculated using the measured pressure P_1 at the inlet pressure tap (see Fig. 1). This is done by assuming homogeneous and incompressible flow in the four short flow paths and their junctions, which separate the pressure tap from the test rod bundle and are meant to minimize the test section entrance effects. The pressure drop associated with each short passage is calculated using sudden-contraction and sudden-expansion approximation with loss coefficients calculated, following the recommendations of Lahey and Moody (1993). A similar approach was used for obtaining the channel exit pressure, P_{out}, using the measured pressure at the exit pressure tap.

In order to maintain the uncertainty associated with the empirical pressure loss coefficients reasonably low, a pressure drop data point was considered reliable only when the sum total of

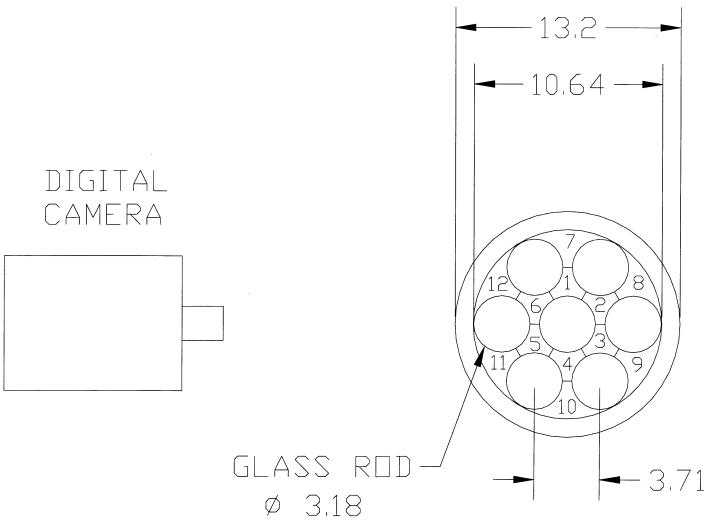

Fig. 2. The micro-rod bundle cross-section.

its inlet and exit irreversible pressure losses was smaller than 20% of the test section total frictional pressure drop, $\Delta P_{f,\,exp}$.

The rod bundle inlet pressure, P_{in}, along with the gas and liquid volumetric mass fluxes, are used as the inlet (initial) conditions for the solution of one-dimensional homogeneous mass and momentum conservation equations representing the flow in the rod bundle. For each test, by inserting any specific correlations for two-phase flow friction in the aforementioned momentum equation, and numerically integrating the mass and momentum conservation equations over the length of the test section, the total frictional pressure drop associated with that correlation could be obtained.

3. Results

3.1. Flow patterns

Six distinct two-phase flow patterns could be identified in the experiments: bubbly, plug/slug, froth, stratified–intermittent, annular–intermittent, and annular–wavy. Representative photographs from each flow pattern are depicted in Fig. 3 where U_{LS} and U_{GS} represent the liquid and gas superficial velocities. The gas and liquid superficial velocity ranges over which the aforementioned flow patterns occurred, are shown in Fig. 4. In all photographs depicting flow patterns, three channels are visible. The inner subchannels 5 and 6 in Fig. 2 are visible through the transparent rod separating them from the camera. The top and bottom channels visible in the photographs are the outer channels 11 and 12 in Fig. 2.

The bubbly flow pattern (Fig. 3a) was characterized by distorted air bubbles with dimensions smaller than the subchannel lateral dimensions. At high gas flow rates (i.e., with high void fraction), the bubbles predominantly accumulated in the peripheral channels, while the central channel appeared to include relatively few air plugs. No gravity-induced stratification, even with respect to the apparent bubble population density, could be noticed in the bubbly flow pattern.

The plug/slug flow patterns, depicted in Fig. 3b, were characterized by elongated bubbles or large gas plugs, occurring in all subchannels visible in the photographs, without noticeable stratification. The liquid phase is clearly continuous in this flow pattern. Slug and plug flow patterns could occur in different subchannels simultaneously, therefore the two flow patterns will not be separately considered.

Froth flow (Fig. 3c), characterized by the absence of a discernible gas–liquid interphase geometric configuration, and in most cases by the occurrence of intermittent discontinuities in both phases, occurred when gas and liquid superficial velocities were both relatively high. In froth flow, the inner subchannels (subchannel 5 and 6 in Fig. 2) could support the slug or plug flow patterns.

The stratified–intermittent flow pattern (Fig. 3d) is a partially-stratified flow pattern, in which the upper subchannels in the test section support an intermittent (plug or slug) flow pattern, while some of the bottom subchannels carry essentially single-phase liquid. The two-phase flow field in micro-rod bundles is evidently sensitive to channel orientation with respect to gravity. As in larger rod bundles (Aly, 1981; Krishnan and Kowalski, 1984; Osamusali et

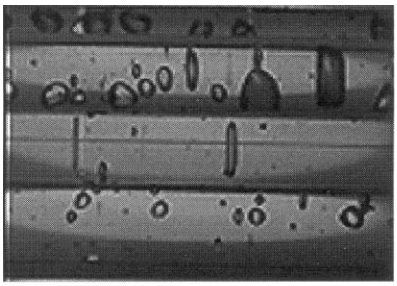

3a. U_{LS}=1.59 m/s
U_{GS}=0.10 m/s

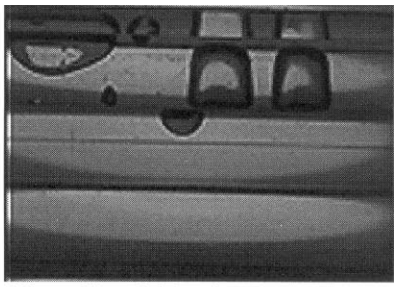

3d. U_{LS}=0.46 m/s
U_{GS}=0.13 m/s

3b. U_{LS}=0.06 m/s
U_{GS}=0.89 m/s

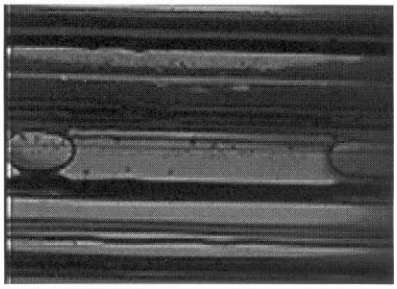

3e. U_{LS}=0.03 m/s
U_{GS}=8.90 m/s

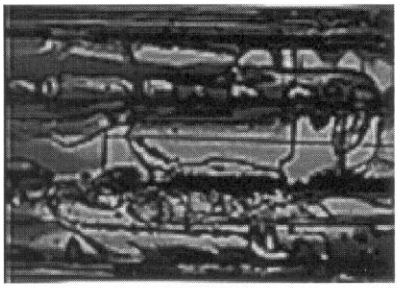

3c. U_{LS}=1.22 m/s
U_{GS}=1.48 m/s

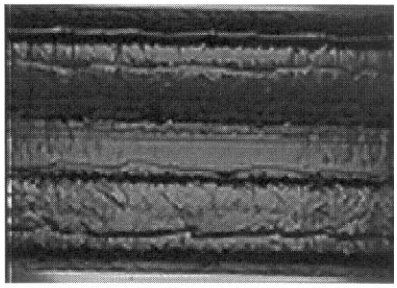

3f. U_{LS}=0.04 m/s
U_{GS}=36.85 m/s

U_{GS}=14.54 m/s

Fig. 3. Representative photographs of flow patterns. (a): bubbly, (b): plug/slug, (c): froth, (d): stratified–intermittent, (e): annular–intermittent, (f): annular.

al., 1992), partial stratification occurs over a wide range of superficial velocities, and can evidently lead to dry out and critical heat flux in heated micro-rod bundles.

The occurrence of partial stratification in micro-rod bundles is an important distinction between the micro-rod bundles and single capillaries. Due to the predominance of surface tension, stratification does not occur in single capillaries similar in hydraulic diameter to our micro rod bundle, and their two-phase flow fields are insensitive to orientation with respect to gravity (Suo and Griffith, 1964; Damianides and Westwater, 1988; Fukano and Kariyasaki, 1993). The two-phase flow regime transitions leading to the development of the stratified–intermittent flow pattern may thus be crucially important for the design and operation of heated micro-rod bundles. Complete stratification, nevertheless, did not occur in the experiments with the micro-bundle even at extremely low gas and liquid flow rates.

The annular–intermittent flow pattern, depicted in Fig. 3e, is a partially-separated flow pattern which has not been reported in single channels. In this flow pattern, the inner subchannels (subchannels 5 and 6 in Fig. 2) supported an intermittent (slug or plug) or froth

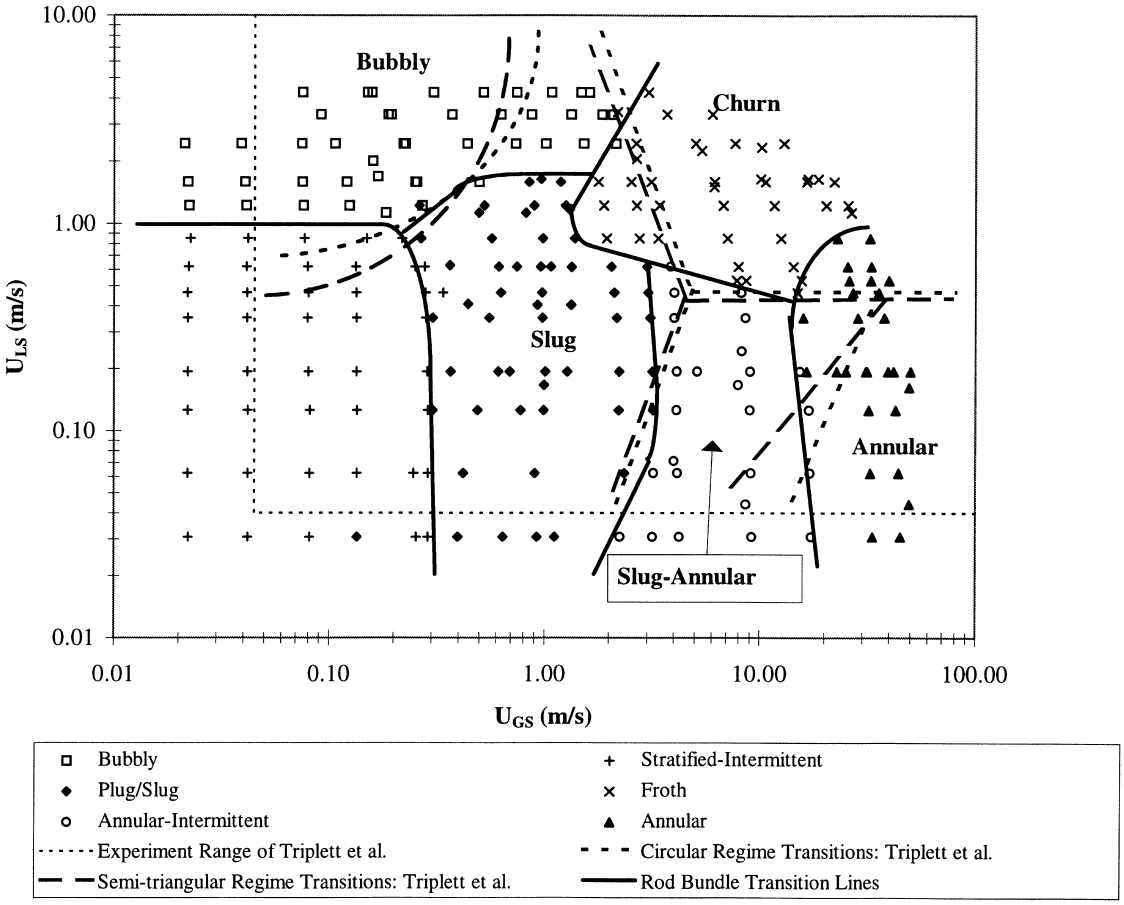

Fig. 4. Flow regimes and flow regime transition lines in the micro-rod bundle, and in the circular and semi-triangular single channels of Triplett et al. (1999a).

flow pattern, while the flow regime in the outer subchannels (subchannels 11 and 12 in Fig. 2) was predominantly annular. The annular–wavy flow pattern, represented by Fig. 3f was characterized by predominantly separated phases in all the channels in the test section and the occurrence of a liquid film on all rods, as well as on the test section tube inner surfaces.

Surface tension is known to effectively suppress the buoyancy effect and any significant interfacial velocity slip, at least in non-separated flow patterns (Fukano and Kariyasaki, 1993). The gravitational force can be assumed to be insignificant in comparison with the surface tension force when (Bretherton, 1961):

$$(\rho_L - \rho_G) g \frac{D_H^2}{\sigma} \ll 1 \tag{1}$$

where D_H is the channel hydraulic diameter. Criteria for the insignificance of buoyancy in comparison with surface tension, the satisfaction of which leads to the impossibility of flow stratification, and the insensitivity of flow patterns to channel orientation, have also been proposed by Suo and Griffith (1964), Barnea et al. (1983) and Brauner and Moalem-Maron (1992). The inequality represented by Eq. (1), as well as all the latter criteria are satisfied in our experiments, as well as other similar studies which have dealt with two-phase flow in single microchannels (Suo and Griffith, 1964; Fukano and Kariyasaki, 1993; Inasaka et al., 1989). The effect of channel orientation was generally insignificant in the aforementioned experiments dealing with single microchannels and consequently stratified flow was not observed in those experiments. The occurrence of partially stratified (annular–intermittent and stratified–intermittent) flow patterns in the micro-rod bundle, however, is indicative of an important buoyancy effect, suggests dependence on orientation, and indicates that the aforementioned criteria may not apply to rod bundles.

3.2. Comparison with flow patterns in single microchannels and large rod bundles

Previous investigations have shown that all major two-phase flow patterns commonly observed in large channels, except for the stratified flow pattern, also occur in single microchannels. The ranges of parameters over which each flow pattern occurs in microchannels, however, disagree with flow regime maps representing large channels rather significantly (Triplett et al., 1999a). A comparison between the flow pattern data obtained in this study and the flow regime map of Mandhane et al. (1974) also showed poor agreement.

The micro-rod bundle flow patterns and their ranges of occurrence, are compared with the experimental data of Triplett et al. (1999a), representing their 1.1 mm diameter circular and 1.09 mm-hydraulic diameter semi-triangular test sections in Fig. 4, using gas and liquid superficial velocities as coordinates. The flow regime maps, representing circular and semi-triangular single microchannels (Triplett et al., 1999a) are evidently similar, with relatively minor differences with respect to flow regime transition lines representing the establishment of bubbly flow, and the slug–annular to annular flow transition. Some similarity between the flow patterns in the micro-rod bundle and the single microchannels can also be observed in Fig. 4. The three flow regime maps are in fair agreement with respect to the ranges of occurrence of annular, and churn or froth flow patterns. Furthermore, the range of occurrence of the slug-annular flow pattern in the single microchannels (a flow pattern represented by annular flow in

long segments of the channel, and interrupted by large-amplitude solitary waves) coincides with the range of occurrence of the annular–intermittent flow pattern in the micro-rod bundle, and the plug/slug and the stratified–intermittent flow patterns in the micro-rod bundle are replaced everywhere with the slug flow pattern in the single microchannels. Thus, the single microchannel data may be useful for the estimation of flow regime transitions representing the establishment of the annular, froth, and annular–intermittent flow patterns in small micro-rod bundles. The conditions leading to the establishment of the crucial partially-stratified (stratified–intermittent) flow pattern in the micro-rod bundle, however, can in no way be deduced from the single microchannel flow patterns.

Aly (1981) and more recently Osamusali et al. (1992) have reported on experiments addressing air–water two-phase flow patterns in the MR-2 test rig. The MR-2 test rig includes a transparent horizontal test section with 10.34 cm inner diameter and 2.44 m long, and contains four 37-rod bundles, each 50 cm long, configured in a series. Aly (1981) and Osamusali et al. (1992) visually identified the flow regimes in their experiments. Osamusali et al. (1992) also utilized a twin-needle fiber optic probe for the measurement of the time-averaged void fraction distributions in their experiments. The flow regime transition data reported by Aly (1981) and Osamusali et al. (1992) are in disagreement with respect to the conditions leading to the establishment of the annular flow regime. The experimental flow regime transition lines of Osamusali et al., however, are reportedly based on a large number (about 225) of data points obtained with aligned bundles, and will be used for comparison with our data here. The flow patterns of Osamusali et al. (1992) are compared with our micro-rod bundle data in Fig. 5. The flow pattern transition lines are evidently different. The occurrence of stratified smooth and stratified wavy flow patterns in the larger rod bundle, and the complete absence of the latter flow patterns in the micro-rod bundle, are the most significant differences between the two flow regime maps.

Krishnan and Kowalski (1984) performed air–water experiments using a test section 50.8 mm in diameter, and containing six horizontal 7-rod bundles with 12.7 mm rods, each 0.6 m long, and configured in series. They focused on the measurement and correlation of void fractions and the hydrodynamic conditions leading to transition to stratified flow. They correlated the latter transition by empirically adjusting a constant in the mechanistic model of Taitel and Duckler (1976). In their experiments, transition to stratified flow occurred over the relatively wide 0.3 m/s $\leq U_{GS} \leq$ 11 m/s range of gas superficial velocity, everywhere at U_{LS}, the liquid superficial velocity, values which agreed relatively well with the experimental results of Osamusali et al. (1992). Evidently, bundle-wide flow stratification can readily occur in large rod bundles. In micro-rod bundles, however, complete stratification, bundle-wide or in separate subchannels, may not occur at all.

3.3. Empirical correlations for flow pattern transitions

Empirical flow regime maps using void fraction, α, and the test section mixture mass flux, G_{TS}, as coordinates in a two-dimensional map provide a simple and convenient method for the selection of appropriate closure relations needed for the solution of two-phase conservation equations, and are widely applied in thermal–hydraulic system codes (Pasamehmetoglu et al., 1990; RELAP5 Development Team, 1995; Paulson et al., 1996). Fig. 6 depicts the flow patterns

representing the micro-rod bundle data. Everywhere in these figures, the void fraction, α, has been calculated using the homogeneous flow assumption:

$$\alpha = \left(\frac{\dot{m}_G/\rho_G}{(\dot{m}_G/\rho_G) + (\dot{m}_L/\rho_L)} \right) \tag{2}$$

where $\dot{m}_G$ and $\dot{m}_L$ are the gas and liquid mass flow rates, respectively. Triplett et al. (1999b) showed that the homogeneous flow assumption provided a reasonable estimate of experimentally measured void fractions in their circular test section, except for churn, wavy–annular and annular flow patterns. Thus, in view of the effective suppression of velocity slip in well-mixed flow patterns in microchannels by surface tension, the predictions of Eq. (2) may be realistic, at least for bubbly and slug/plug flow patterns. For the micro-rod bundle, for $\alpha < 0.25$, the bubbly to stratified–intermittent transition boundary can be represented by:

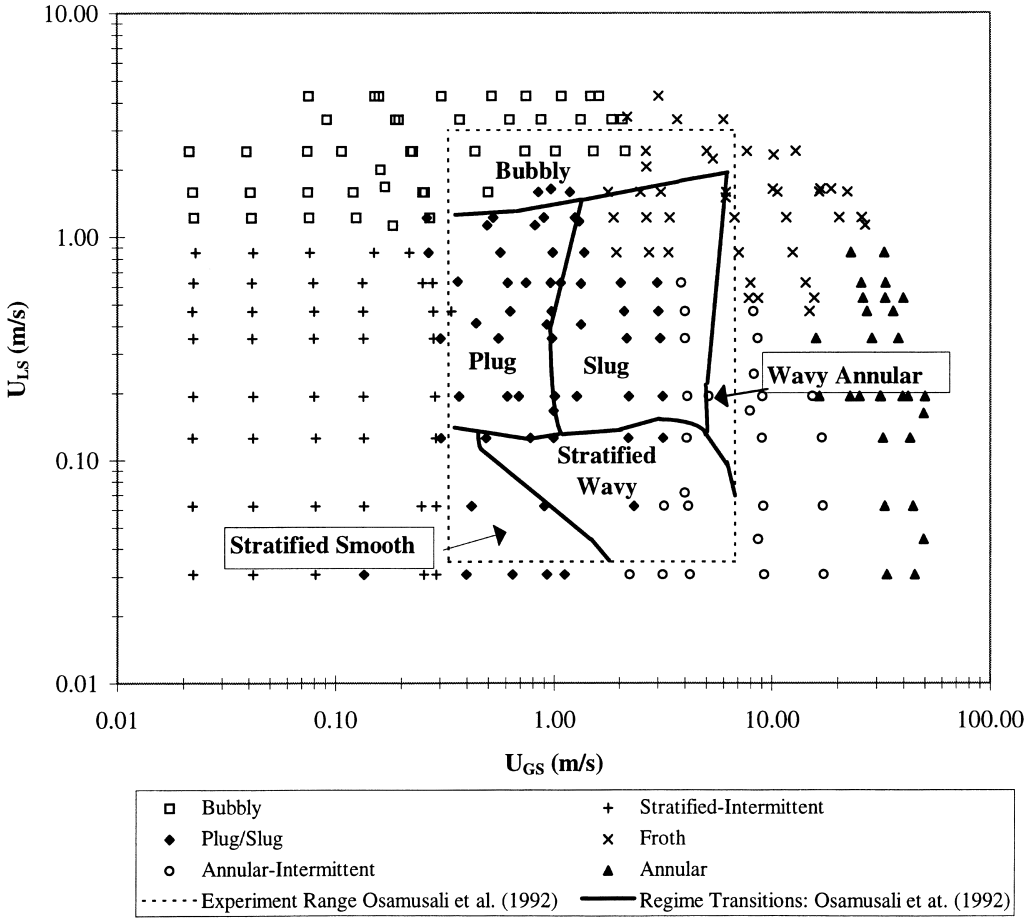

Fig. 5. Comparison of the flow patterns in the micro-rod bundle with flow patterns in the large horizontal rod bundle of Osamusali et al. (1992).

$$G_{TS} = 1000 \text{ kg/m}^2\text{s} \tag{3}$$

For $0.25 < \alpha < 0.8$, the boundary between stratified–intermittent and plug/slug flow patterns follows:

$$\ln G_{TS} = -4.7\alpha + 8.1 \tag{4}$$

The flow regime transition lines leading to the establishment of wavy–annular and annular flow patterns are not correlated in terms of G_{TS} and α, since the homogeneous flow assumption is generally inadequate for the latter flow patterns. A reasonable lower limit for the establishment of the latter flow patterns, nevertheless, can be $\alpha = 0.8$, for points below the curve represented by Eq. (4).

3.4. Pressure drop

Typical pressure drop data are provided in Table 1. The experimental pressure drop data were compared with the predictions of the homogeneous flow model based on McAdams (1954) correlation for two-phase viscosity, and Friedel's (1979) correlation. The statistical characteristics of the model-data comparisons can be understood by calculating parameters

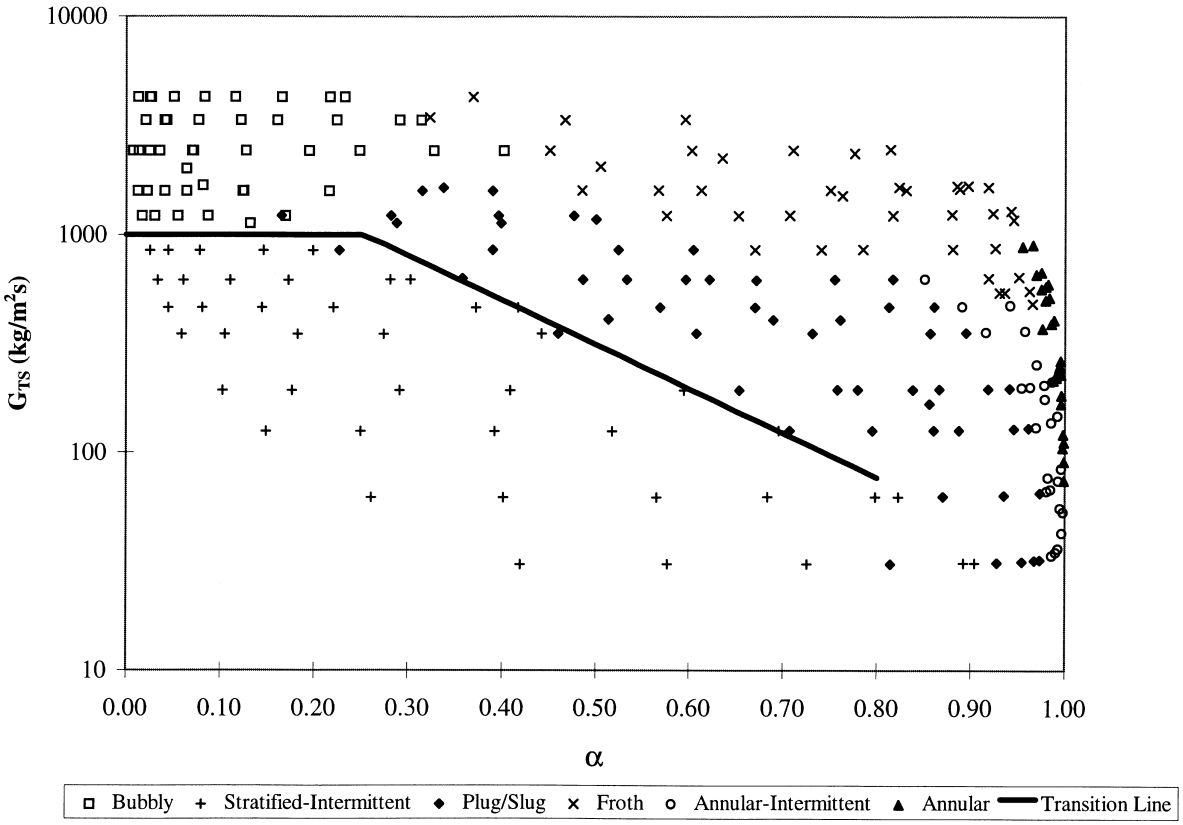

Fig. 6. Flow pattern transition lines in the micro-rod bundle.

ξ_{mean} and σ_{ξ}, which represent the mean and standard deviation of the following statistic:

$$\xi = 100\left[\frac{\Delta P_{f,\,model} - \Delta P_{f,\,exp}}{\Delta P_{f,\,model}}\right] \tag{5}$$

Table 1
Summary of pressure drop data

U_{LS} (m/s)	U_{GS} (m/s)	P_{in} (kPa)	$\Delta P_{f,\,exp}$ (kPa)	U_{LS} (m/s)	U_{GS} (m/s)	P_{in} (kPa)	$\Delta P_{f,\,exp}$ (kPa)
1.13	0.17	127.3	16.1	0.62	0.13	116.7	5.8
1.13	0.76	132.9	20.5	1.59	0.11	136.3	25.6
1.64	0.86	152.9	39.8	3.35	0.07	202.9	91.6
2.01	0.14	153.9	43	1.22	0.49	134.3	22.6
2.06	2.2	196.5	81.6	1.22	1.14	141.1	29.7
1.64	16.11	236	127.2	1.59	0.23	146.1	34.2
0.17	0.99	114.9	3.3	1.59	1.05	152.8	41.1
0.41	0.43	116.8	4.6	2.43	0.18	177.6	66.1
0.41	1.3	119.9	7.1	2.43	0.59	190.9	78.5
0.62	0.72	122.5	10.4	3.35	0.15	220.8	109.1
0.62	1.28	124.3	12.3	3.35	0.48	234.1	121.4
0.03	0.25	113	0.7	1.5	6.88	143.3	31.3
0.03	0.64	113.7	0.7	2.33	16.03	180.5	69
0.03	1.12	113	0.7	0.62	5.87	177.3	65.1
0.06	0.42	113	1.4	1.22	1.98	234.2	123.2
0.13	0.3	113.7	1.3	0.85	0.15	117	6.3
0.13	0.77	114.3	2	0.85	0.55	122.1	10.2
0.19	0.37	113.6	2	0.85	1.32	124.2	13.2
0.19	1	114.9	2.6	0.13	3.15	115.4	3.2
0.35	0.55	116.9	4.6	0.35	3.01	120.8	8.2
0.46	0.33	117.5	5.2	0.62	2.82	128.8	17.2
0.46	0.95	118.6	7.1	1.59	6.75	152	40.5
0.62	0.59	121.2	9.8	3.35	0.76	210.3	97.2
0.03	0.13	113	0.7	0.06	2.33	108.1	1.3
0.13	0.13	113	0.7	0.19	2.18	115.3	4.5
0.35	0.13	114.2	2.6	0.46	2.03	123.6	10.2
0.46	2.03	123.6	10.2	3.35	3.46	127.9	16.6
1.59	28.08	142.5	30.2	2.43	2.21	163.8	52.6
2.43	2.92	160.3	47.6	4.28	3.3	135.8	25.5
0.03	0.29	113	0.7	0.85	0.02	119.1	8.4
0.13	0.29	113.7	1.3	0.46	0.02	114.9	4
0.35	0.28	115.6	3.3	0.19	0.02	113	1.3
0.62	0.27	118.7	7.2	0.06	0.02	113	0.7
1.22	0.25	131.1	20	0.03	0.04	113	0.7
4.28	0.67	169.7	58.7	0.13	0.04	113	0.7
0.03	0.08	113	0.7	0.35	0.04	115	2.6
0.13	0.08	113	1.4	0.62	0.04	116.7	5.9
0.35	0.08	114.9	2.6	3.35	2.1	127.2	16.7
0.62	0.08	116.7	5.9	1.59	0.2	162.5	51.4

The results were strongly flow regime-dependent. At very low liquid superficial velocities, the data were scattered rather widely, suggesting unsteady and chaotic flow patterns. The data scatter was particularly large for the annular–intermittent flow regime. Except for plug/slug and annular–intermittent flow patterns at low U_{LS}, the homogeneous mixture model generally under predicted the data. The under prediction of annular flow data was particularly significant. Friedel's correlation (Friedel, 1979) appeared to better compare with the experimental data. For the data representing low U_{LS}, where wide scatter can be noted, Friedel's correlation over predicted the data, and it systematically under predicted the data at high U_{LS}. With the homogeneous flow model, for the entire data set, $\xi_{mean} \approx -42\%$ and $\sigma_{\xi} \approx 2.7\%$ were obtained. The correlation of Friedel (1979) predicted the data with $\xi_{mean} \approx 66\%$ and $\sigma_{\xi} \approx 11.6\%$.

4. Concluding remarks

Gas–liquid two-phase flow patterns and frictional pressure drops in a horizontal rod bundle were experimentally investigated in this work. The rod bundle consisted of 7 rods, 23-cm long and 3.18-mm in diameter, arranged in a triangular array with a 3.71-mm pitch. The rod bundle was entirely transparent, allowing for visual identification of flow patterns.

Six distinct flow patterns could be identified in the tests: bubbly, plug/slug, froth, stratified–intermittent, annular–intermittent and annular. In the stratified–intermittent flow pattern, the bottom subchannels supported single-phase liquid flow, while bubbly or plug/slug flow patterns occurred in one or more of the subchannels near the bundle top. In the annular–intermittent flow pattern, the two-phase flow regime in some subchannels was bubbly or plug/slug, while other subchannels were in annular flow. The flow regimes and their ranges of occurrence were different from previously reported experiments representing horizontal large rod bundles. The major flow regime transition lines were empirically correlated as functions of mass flux and void fraction, with the latter obtained, assuming homogeneous flow.

The frictional pressure drops were sensitive to the two-phase flow pattern. The data were compared with the predictions of the homogeneous mixture model, and the empirical correlation of Friedel (1979). Neither correlation could satisfactorily predict the data over the entire flow regime map. Except for data representing annular–intermittent and plug/slug flow patterns at low liquid superficial velocities, the homogeneous mixture model consistently and significantly under predicted the frictional pressure drops. The correlation of Friedel (1979) predicts most of the experimental data typically within a factor of 2, except for data representing very low liquid superficial velocities.

References

Aly, A.M.M., 1981. Flow regime boundaries for an interior subchannel of a horizontal 37 element bundle. Can. J. Chem. Eng 59, 158–163.

Amos, C.N., Schrock, V.E., 1984. Two-phase critical flow in slits. Nucl. Sci. Eng 88, 261–274.

Bao, Z.Y., Bosnick, M.G., Haynes, G.S., 1994. Estimation of void fraction and pressure drop for two-phase flow in fine passages. Trans. Inst. Chem. Eng 72, 625–632.

Barnea, D., Luninski, Y., Taitel, Y., 1983. Flow in small diameter pipes. Can. J. Chem. Eng 61, 617–620.
Brauner, N., Moalem-Maron, D., 1992. Identification of the range of 'small diameter' conduits regarding two-phase flow pattern transitions. Int. Comm. Heat Mass Transfer 19, 29–39.
Bretherton, F.P., 1961. The flow of long bubbles in tubes. J. Fluid Mech 10, 166–188.
Damianides, C.A., Westwater, J.W., 1988. Two-phase flow patterns in a compact heat exchanger and in small tubes. In: Proceedings of the Second UK National Conf. on Heat Transfer, Glasgow, September 14–16, 1257–1268.
Friedel, L., 1979. Improved pressure drop correlation for horizontal and vertical two-phase flow. 3 R International 18, 485–492.
Fukano, T., Kariyasaki, A., 1993. Characteristics of gas–liquid two-phase flow in a capillary. Nucl. Eng. Des 141, 59–68.
Geng, H., Ghiaasiaan, S.M., 1998. Mechanistic non-equilibrium modeling of critical flashing flow of subcooled liquids containing dissolved noncondensables. Nuclear Sci. Eng 129, 294–304.
Ghiaasiaan, S.M., Muller, J.R., Sadowski, D.L., Abdel-Khalik, S.I., 1997. Critical flow of initially highly subcooled water through a short capillary. Nucl. Sci. Eng 126, 229–238.
Inasaka, F., Nariai, H., Shimura, T., 1989. Pressure drops in subcooled flow boiling in narrow tubes. Heat Transfer Japanese Research 18, 70–82.
John, H., Reimann, J., Wesphal, F., Friedel, L., 1988. Critical two-phase flow through rough slits. Int. J. Multiphase Flow 14, 155–174.
Krishnan, V.S., Kowalski, J.E., 1984. Stratified-slug flow transition in a horizontal pipe containing a rod bundle. AIChE Symp. Series 80 (236), 282–289.
Lahey Jr, R.T., Moody, F.J., 1993. The Thermal-Hydraulics of a Boiling Water Nuclear Reactor, 2nd ed. American Nuclear Society, LaGrange Park, IL.
Mandhane, J.M., Gregory, G.A., Aziz, K., 1974. A flow pattern map for gas–liquid flow in horizontal pipes. Int. J. Multiphase Flow 1, 537–553.
McAdams, W.H., 1954. Heat Transmission, 3rd ed. McGraw-Hill, New York.
Narrow, T.L., 1998. Flow Visualization within a seven-rod micro-bundle. MS Thesis, Georgia Institute of Technology, Atlanta, GA.
Osamusali, S.E., Groeneveld, D.C., Cheng, S.C., 1992. Two-phase flow regimes and onset of flow stratification in horizontal 37-rod bundles. Heat and Technology 10, 46–74.
Oya, T., 1971. Upward liquid flow in small tube into which air streams. Bulletin of the JSME 14, 1320–1339.
Pasamehmetoglu, K.O. et al., 1990. TRAC-PFI/MOD2 Theory Manual. Los Alamos National Laboratory, Los Alamos, NM.
Paulson, M.P., et al., 1996. RETRAN-3D — A program for transient analysis of complex fluid flow systems. Vol. 1: Theory Manual. EPRI NP-7450. Electric Power Research Institute, Palo Alto, CA.
Peng, X.F., Wang, B.X., Peterson, G.P., Ma, H.B., 1995. Experimental investigation of heat transfer in flat plates with rectangular microchannels. Int. J. Heat Mass Transfer 38, 127–137.
RELAP5 Development Team, 1995. RELAP5/MOD3 Code Manual. Vol. 1: Code Structure, System Models and Solution Methods. NUREG/CR-5535, INEL-95/0174, Idaho National Engineering and Environmental Laboratory, ID.
Suo, M., Griffith, P., 1964. Two-phase flow in capillary tubes. J. Basic Eng 86, 576–582.
Taitel, Y., Duckler, A.E., 1976. A model for predicting flow regime transition in horizontal and near horizontal gas liquid flow. AIChE J 22, 47–55.
Triplett, K.A., Ghiaasiaan, S.M., Abdel-Khalik, S.I., Sadowski, D.L., 1999a. Gas–liquid two-phase flow in microchannels. Part I: Two-phase flow patterns. Int. J. Multiphase Flow 25, 377–394.
Triplett, K.A., Ghiaasiaan, S.M., Abdel-Khalik, S.I., Lemouel, A., McCord, B.N., 1999b. Gas–liquid two-phase flow in microchannels. Part II: Void fraction and pressure drop. Int. J. Multiphase Flow 25, 395–410.
Ungar, E.K., Cornwell, J.D., 1992. Two-phase pressure drop of ammonia in small diameter horizontal tubes. In: AIAA 17th Aerospace Ground Testing Conf., Nashville, TN, 6-8.